Neurobiology of Disease 214 (2025) 107051

Contents lists available at ScienceDirect

Neurobiology of Disease

journal homepage: www.elsevier.com/locate/ynbdi

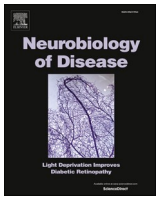

Circulating mitochondrial components and metabolic and inflammatory markers in Charcot-Marie-Tooth type 2B

Giulia Girolimetti [a], Federico Marini [b], Riccardo Calvani [c,d], Hélio José Coelho-Júnior [c], Jacopo Gervasoni [c], Lavinia Santucci [c], Stefano Tozza [e], Fiore Manganelli [e], Paola Saveri [f], Davide Pareyson [f], Emanuele Marzetti [c,d,*], Cecilia Bucci [a,**], Anna Picca [c,g,1], Flora Guerra [h,1]

[a] Department of Experimental Medicine (DiMeS), University of Salento, Lecce, Italy
[b] Department of Chemistry, University of Rome "La Sapienza", Rome, Italy
[c] Fondazione Policlinico Universitario "Agostino Gemelli" IRCCS, Rome, Italy
[d] Department of Geriatrics, Orthopedics and Rheumatology, Università Cattolica del Sacro Cuore, Rome, Italy
[e] Department of Neuroscience, Reproductive Sciences and Odontostomatology, University of Naples "Federico II", Naples, Italy
[f] Department of Clinical Neurosciences, Fondazione IRCCS Istituto Neurologico Carlo Besta, Milan, Italy
[g] Department of Medicine and Surgery, LUM University, Casamassima, Italy
[h] Department of Biological and Environmental Sciences and Technologies (DiSTeBA), University of Salento, Lecce, Italy

ARTICLE INFO

Keywords:
Biomarker
Cytokine
Damage-associated molecular patterns
Inflammation
Mitochondrial quality
Mitophagy
Multi-marker

ABSTRACT

Charcot-Marie-Tooth type 2B (CMT2B) is a rare inherited neuropathy caused by mutations in the *RAB7A* gene. Altered mitochondrial dynamics and late endosome trafficking contribute to CMT2B pathophysiology. In this case-control study, we quantified levels of circulating cell-free mtDNA (ccf-mtDNA), mitochondrial proteins secreted within mitochondria-derived vesicles (MDVs), and metabolic and inflammatory markers in biofluids of individuals with CMT2B ($n = 5$) and healthy controls ($n = 4$). ccf-mtDNA was quantified in serum by droplet digital PCR. MDVs were purified by immunoprecipitation and analyzed by Western blotting. A panel of 27 inflammatory markers was assayed in serum by multiplex immunoassay. Forty-four amino acids and derivatives were quantified in serum and urine by ultraperformance liquid chromatography/mass spectrometry (UPLC/MS). Fourteen long-chain fatty acids and asymmetric dimethyl arginine (ADMA) were measured in serum by UPLC/MS. Analysis of variance – simultaneous component analysis models were built to explore differences in metabolic and inflammatory markers between cases and controls. Mann–Whitney *U* test was used to compare ccf-mtDNA levels between groups. Spearman's correlation analysis was applied to explore the relationship between markers of inflammation, endothelial dysfunction, and fatty acid metabolism. CMT2B participants had higher levels of ADMA as well as of interleukin (IL)-1b, IL-8, IL-9, IL-13, eotaxin, and most fatty acids than controls. Serum levels of 1- and 3-methylhistidine, alfa- and beta-aminobutyric acid, asparagine, glycine, threonine, and fibroblast growth factor were lower in CMT2B samples than in controls. No significant differences were observed for ccf-mtDNA levels between groups, while differences in MDV content were identified between participants with CMT2B and controls. Among the metabolic markers, ADMA was the most discriminant biomolecule distinguishing CMT2B participants from controls and showed a positive correlation with some fatty acids. Collectively, these findings suggest that CMT2B may be associated with altered endosomal trafficking and mitochondrial and endothelial dysfunction.

1. Introduction

Charcot-Marie-Tooth (CMT) is a rare inherited neurodegenerative disease that affects the peripheral nervous system and encompasses a variety of clinical, electrophysiological, pathological, and genetic phenotypes (Pareyson and Marchesi, 2009). This neuropathy can be caused

* Corresponding author at: Fondazione Policlinico Universitario "Agostino Gemelli" IRCCS, Rome, Italy.
** Corresponding author.
E-mail addresses: emanuele.marzetti@unicatt.it (E. Marzetti), cecilia.bucci@unisalento.it (C. Bucci).
[1] Anna Picca and Flora Guerra equally contributed to this work as senior authors.

https://doi.org/10.1016/j.nbd.2025.107051
Received 12 March 2025; Received in revised form 4 August 2025; Accepted 5 August 2025
Available online 6 August 2025

by alterations in more than 100 genes, many of which are involved in the regulation of membrane trafficking (Bucci et al., 2012; Pareyson and Marchesi, 2009).

Among the different CMT subtypes, CMT type 2B (CMT2B) is a dominant, axonal form that can be caused by six missense mutations (p.L129F, p.K157N, p.N161T/I, p.V162M, and p.K126R) in the *RAB7A* gene which encodes a GTPase of the RAB family (Bucci et al., 1988; Chavrier et al., 1990; Houlden et al., 2004; Meggouh et al., 2006; Saveri et al., 2020; Verhoeven et al., 2003; Wang et al., 2014). Prominent sensory loss, progressive distal weakness leading to atrophy, reduced tendon reflexes, and normal or near-to-normal nerve conduction velocities are specific characteristics of CMT2B (Bucci et al., 2012; Manganelli et al., 2012; Tazir et al., 2014), although a recently described case with p.K126R mutation showed a severe axonal motor-sensory polyneuropathy (Saveri et al., 2020). CMT2B is also classified as an ulcer-mutilating neuropathy because patients manifest other signs such as foot deformities and high frequency of ulcers and infections leading to toe and foot amputations (Bucci et al., 2012; Manganelli et al., 2012; Tazir et al., 2014), except for patients with p.K126R mutation (Saveri et al., 2020).

CMT is incurable and only a few therapeutic options are available, including physical therapy, occupational therapy, orthopedic surgery, and/or device implantation (Dong et al., 2024). Mounting evidence highlights the relevance of immune regulation in neurodegeneration (Mayne et al., 2020). Neurodegenerative diseases are a large group of disorders affecting specific subsets of neurons and are characterized by heterogeneous clinical and pathological features. Common neurodegenerative diseases, like Alzheimer's disease, Parkinson's disease, amyotrophic lateral sclerosis, frontotemporal dementia, and Huntington's disease, develop upon the common background of chronic neuroinflammation (Mayne et al., 2020). In most cases, this inflammatory milieu arises from a state of chronic sterile inflammation linked, at least partly, to mitochondrial dysfunction (Picca et al., 2020a, 2020b). In the context of compromised mitochondrial quality, immune receptors of microglia recognize mitochondrial-derived damage-associated molecular patterns (DAMPs) (e.g., mtDNA, mitochondrial unfolded protein response molecules, mitochondrial reactive oxygen species, ATP, mitochondrial transcription factor A, cardiolipin, cytochrome C, mitochondrial calcium and iron) thereby inciting neuroinflammation (Ferrucci et al., 2024; Lin et al., 2022). Furthermore, the intracellular signaling cascade induced by inflammatory mediators regulates mitochondrial metabolism and function. Indeed, mitochondrial dysfunction precedes neuroinflammation during disease progression (Lin et al., 2022).

RAB7A mutations have recently been associated with alterations of mitochondrial dynamics (Gu et al., 2022; Wong et al., 2019) and changes in lipid metabolism in CMT2B patients (Giudetti et al., 2020). Moreover, RAB7, by controlling the fusion of mitochondria-derived vesicles (MDVs) with late endosomes for their subsequent degradation (Matheoud et al., 2016), is thought to be responsible for the mitochondrial antigen-presenting system in immune cells via MDV trafficking in the absence of the mitophagy regulators PTEN-induced kinase 1 (PINK1) or Parkin (Matheoud et al., 2016). We have also demonstrated that RAB7 is a key regulator of MDV secretion (Gagliardi et al., 2024). Among its multiple functions, RAB7 also regulates mitophagy (Yamano et al., 2014), and the autophagy machinery was found to be impaired in fibroblasts from CMT2B patients (Colecchia et al., 2018; Romano et al., 2022). An excessive accumulation of mitochondrial DAMPs, such as mtDNA, also in an oxidized form, and oxidized cardiolipin, can be a consequence of impaired mitophagy. MDVs can shuttle mitochondrial DAMPs, and/or be DAMPs themselves. On the other hand, cell-free mtDNA (cf-mtDNA), lacking histones and having hypomethylated CpG motifs, can be recognized by a set of receptors of innate immunity as "non-self", likely because of its bacterial DNA ancestry, thereby triggering inflammation (Kepp et al., 2011).

Based on these premises, we decided to investigate secreted MDVs as well as circulating cf-mtDNA (ccf-mtDNA) levels along with metabolic and inflammatory markers in biofluids of CMT2B patients to 1) verify whether high levels of ccf-mtDNA and MDVs characterize CMT2B patients; and 2) define a mitochondrial and metabolic profile of the disease that may shed light onto its pathogenic mechanisms.

2. Materials and methods

2.1. Study design and participants

We conducted a case-control study in five patients with CMT2B and four healthy controls. Participants were anonymized according to protocols approved by the Ethics Committee of Azienda Ospedaliera Universitaria "Federico II" (Naples, Italy; protocol # 107/05) and the National Institute of Health (NIH) Ethics Committee (NIH INC 6601 BST 14–10, date of approval 15 December 2021). Four patients harbored *RAB7A* p.V162M mutation and were named CMT2B_1 to 4. One patient carried *RAB7A* p.K126R mutation and was labeled as CMT2B_5. Healthy donors were renamed Ctrl1 to 4. The study was conducted in accordance with the ethical standards laid down in the 1964 Declaration of Helsinki and its later amendments. All participants gave their informed consent prior to the inclusion in the study.

2.2. Blood and urine collection and processing

Blood samples for serum separation were collected after overnight fasting using commercial tubes. Upon collection, blood samples were kept for 30 min at room temperature for clotting and then centrifuged at 1100 $\times g$ for 15 min at 4 °C. The upper clear fraction (serum) was collected in 0.5 mL aliquots and stored at −80 °C for later use. First-void urine samples (5 mL per participant) were collected in sterile polypropylene tubes. Upon delivery, urine samples were centrifuged at 1500 rpm for 15 min at 4 °C. The supernatant was collected and stored at −80 °C until analysis.

2.3. Circulating cell free mitochondrial DNA copy number quantification by droplet digital PCR (ddPCR)

Copy number of ccf-mtDNA was quantified in serum collected from each patient at the time of diagnosis and from controls using ddPCR as described by Podlesniy and Trullas (2018). All reagents, consumables, and instruments were purchased from Bio-Rad Laboratories (Hercules, CA, USA). 2 × ddPCR Supermix for Probes (No-dUTP), 0.9 μM (final concentration) of mtDNA forward primer (mtDNA-85F 5′-CTCACTCCTTGGCGCCTGCC-3′), 0.9 μM (final concentration) mtDNA reverse primer (mtDNA-85R 5′-GGCGGTTGAGGCGTCTGGTG-3′), 0.1 μM hydrolysis probe (FAM-5′-CCTCCAAATCACCA-CAGGACTATTCCTAGCCATGCA-3′-BHQ-1, BHQ1, Black Hole Quencher-1; FAM, 6-carboxyfluorescein), and 1 μL of undiluted serum sample as the mtDNA template source were used and assembled in a 20 μL reaction. The reaction mixture was placed in DG8 Cartridge for Droplet Generator together with the ddPCR Droplet Generation Oil for Probes to partition samples into nanoliter-sized droplets using a QX200 Droplet Generator. The resulting emulsified sample (~40 μL) was used to perform a PCR reaction on a T100 Thermal Cycler, using the following conditions: 95 °C for 10 min; 40 cycles of 94 °C, 30 s each; 60 °C for 1 min; 98 °C for 10 min; 4 °C on hold. The ramp rate between all steps was 2 °C/s. The PCR product was placed into a QX200 Droplet Reader to measure fluorescence. Samples with less than 10,000 droplets were not considered for the analysis. Hence, Ctrl1 was excluded. QX200 Droplet Reader uses a detection system for FAM to analyze each droplet individually, providing a direct quantification of target DNA based on PCR-positive and PCR-negative droplet counts. Data were analyzed using Bio-Rad QX Manager 1.2 Standard Edition (Bio-Rad). A threshold for positive droplets based on droplet clustering across all samples against that of a negative serum-free control was set and the concentration of mtDNA in the starting template (copies/μL) for each sample was obtained.

2.4. Determination of serum and urine concentrations of metabolic markers

2.4.1. Measurement of amino acids and derivatives in serum and urine

A panel of 44 amino acids and derivatives were measured in serum and urine samples by ultraperformance liquid chromatography/mass spectrometry (UPLC/MS). The panel included: 1-methylhistidine, 3-methylhistidine, 4-hydroxyproline, α-aminobutyric acid, β-alanine, β-aminobutyric acid, γ-aminobutyric acid, alanine, allo-isoleucine, aminoadipic acid, anserine, arginine, asparagine, aspartic acid, carnosine, citrulline, cystathionine, cystine, ethanolamine, glutamic acid, glutamine, glycine, glycil proline, histidine, homocitrulline, homocystine, hydroxylysine, isoleucine, kynurenine, leucine, lysine, methionine, ornithine, phenylalanine, phosphoethanolamine, proline, sarcosine, serine, sulfocysteine, taurine, threonine, tryptophan, tyrosine, and valine. Each sample was treated following a deproteinization step and a derivatization step using AccQTag reagent (Waters Corporation; Milford, MA, USA). Afterward, samples were loaded onto a CORTECS UPLC C18 column 1.6 μm, 2.1 mm × 150 mm (Waters Corporation) for chromatographic separation (ACQUITY H-Class, Waters Corporation). Elution was accomplished at 0.5 mL/min flowrate with a linear gradient (9 min) from 99:1 to 1:99 water 0.1 % formic acid/acetonitrile 0.1 % formic acid. Analytes were detected on an ACQUITY QDa single quadrupole mass spectrometer equipped with an electrospray source operating in positive mode (Waters Corporation).

2.4.2. Measurement of fatty acids in serum

A panel of 14 long chain fatty acids (α-linolenic, γ-linolenic acid, arachidonic acid, dihomo-γ-linolenic acid, docosahexenoic acid, eicosapentaenoic acid, elaidic acid, linoleic acid, linolelaidic acid, myristic acid, oleic acid, palmitic acid, palmitoleic acid, and stearic acid) was quantified in serum samples through gas chromatography–electron ionization–MS (GC–EI-MS) validated methodology (EUREKA Lab Division KIT, code GC75010; Chiaravalle, AN, Italy). After extraction and washing, samples were derivatized for 15 min at 100 °C. The solution, after various dilutions, was directly injected into the instrument. GC–EI-MS analyses were performed using a Trace GC Ultra (Thermo Fisher Scientific, San Jose, CA, USA) equipped with Durabond HP-88 column with 100 m × 0.25 mm × 0.2 μm film thickness (Agilent, Santa Clara, CA, USA) and connected to a ISQ mass spectrometer (Thermo Fisher Scientific). The chromatographic separation was performed with a temperature gradient: initial oven temperature of 100 °C was held for 1 min, raised to 220 °C at 10 °C/min. Total run time was 30 min. Analyses were performed in selected ion monitoring (SIM) mode.

2.4.3. Measurement of asymmetric dimethyl arginine in serum

Asymmetric dimethyl arginine (ADMA) was measured in serum samples by UPLC/MS-MS, as previously described (Santucci et al., 2023). The UPLC/MS–MS system consisted of an UPLC and autosampler ExionLC AD system (ABSciex, Framingham, MA, USA) and a Qtrap 6500+ (ABSciex) equipped with electrospray ion source. Analyses were conducted in positive ion mode. The analytical procedure requires a deproteinization step, performed by adding 300 μL of methanol containing 0.3 μmol/L of [$^2H_7$] ADMA to 50 μL of sample. The chromatographic separation was performed with a flow rate of 0.45 mL/min using a LUNA HILIC column, 3 μm, 200 Å, 100 × 2.0 mm (Phenomenex, Torrance, CA, USA) with a gradient of mobile phase A (H_2O containing 0.1 % formic acid and 20 mM ammonium formate) and mobile phase B (90 % acetonitrile containing 0.1 % formic acid and 20 mM ammonium formate). The oven temperature was set at 40 °C. The injection volume was 2 μL and the total analysis time was 5.5 min. Analyte detection was performed with an MRM experiment.

2.5. Measurement of inflammatory markers in serum

A panel of 27 inflammatory biomolecules was measured in duplicate in serum with a Bio-Plex Pro Human Cytokine 27-plex Assay kit (#M500KCAF0Y, Bio-Rad) on a Bio-Plex® System with Luminex xMap Technology (Bio-Rad). Inflammatory molecules included in the panel are listed in Table 1. Instrument default settings were used for data acquisition on the Bio-Plex Manager Software 6.1 (Bio-Rad). Before data export, optimization of standard curves across all analytes was performed and outliers were removed.

Table 1
List of inflammatory biomolecules assayed by multiplex immunoassay.

Class	Biomolecules
Cytokines	IFN-γ, IL-1β, IL-1Ra, IL-2, IL-4, IL-5, IL-6, IL-7, IL-8, IL-9, IL-10, IL-12, IL-13, IL-15, IL-17, TNF-α
Chemokines	CCL5, CCL11, IP-10, MCP-1, MIP-1α, MIP-1β
Growth factors	FGF-β, G-CSF, GM-CSF, PDGF-BB, VEGF

Abbreviations: CCL, C—C motif chemokine ligand; FGF, fibroblast growth factor; G-CSF, granulocyte colony-stimulating factor; GM-CSF, granulocyte macrophage colony-stimulating factor; IFN, interferon; IL, interleukin; IL-1Ra, interleukin 1 receptor agonist; IP-10: interferon-induced protein 10; MCP-1, monocyte chemoattractant protein 1; MIP, macrophage inflammatory protein; PDGF-BB, platelet derived growth factor BB; TNF, tumor necrosis factor; VEGF, vascular endothelial growth factor.

2.6. Immunopurification of mitochondria-derived vesicles and Western blot analysis

The immunoisolation protocol for extracellular vesicles (EVs) was performed using the Exosomes Isolation Kit Pan (Miltenyi Biotec, Germany), following the manufacturer's instructions. Purified EVs were lysed in Laemmli Buffer (100 mM Tris–HCl pH 6.8, 4 % SDS, 20 % glycerol, and 0.2 % blue bromophenol). Proteins were separated by sodium dodecyl sulphate polyacrylamide gel electrophoresis (SDS-PAGE) and subsequently electroblotted onto polyvinylidenefluoride (PVDF) Immobilon-P membranes (Millipore, Billerica, MA, USA), as previously described (Romano et al., 2021a). Primary antibodies were incubated overnight followed by a 1 h incubation with anti-mouse and anti-rabbit peroxidase-conjugated secondary antibodies. The purity of EVs was ascertained according to the minimal information for studies of extracellular vesicles (MISEV2023) guidelines (Welsh et al., 2024). The presence of the cytosolic protein, tumor susceptibility gene 101 (TSG101) (ab30871, Abcam, Cambridge, MA, USA), and two tetraspanins, CD63 and CD9 (positive controls; sc-5275, sc-13,118, Santa Cruz Biotechnology, Santa Cruz, CA, USA), as well as the absence of the non-EV component ribosomal protein S6 (RPS6) (negative control; sc-74,459, Santa Cruz Biotechnology), were verified using cellular lysates from SHSY5Y cell lines as expression control. Mitochondrial content of EVs was assessed using antibodies against ATP synthase subunit alpha (ATP5A), succinate dehydrogenase subunit B (SDHB), NADH:ubiquinone oxidoreductase subunit B8 (NDUFB8) (anti-OXPHOS cocktail, ab110413, Abcam), and SDHA (COMPLEX II Antibody Cocktail, ab110410, Abcam). Images were acquired using a ChemiDoc MP Imaging System and analyzed by ImageJ software (Version 1.5Oi, Bethesda, MD, USA). Protein expression levels were quantified by densitometry and normalized against serum total proteins.

2.7. Statistical analysis

The presence of significant differences in metabolic and inflammatory markers between individuals with CMT2B and controls was assessed through analysis of variance (ANOVA) – simultaneous component analysis (ASCA) and common components (CC) and specific weights analysis (also termed Common Dimensions or ComDim analysis). ASCA is the generalization of ANOVA to complex multivariable datasets and is particularly useful when the significance of the effect of one or more controlled factors on multivariate experimental data (with

Table 2
Main clinical characteristics of study participants.

Participant ID	RAB7 amino acid change	Age (years)	Sex	Age at diagnosis (years)	Age of onset (years)	Clinical features
CMT2B_1	V162M	56	M	45	15	Walking difficulty, ulcers, amputation
CMT2B_2	V162M	57	M	50	25	Tendency to stumble, dysautonomia
CMT2B_3	V162M	56	F	42	17	Walking difficulty
CMT2B_4	V162M	58	M	44	17	Ulcers
CMT2B_5	K126R	44	F	36	14	Walking difficulties, progressive distal muscle wasting and weakness
Ctrl1	–	55	M	–	–	–
Ctrl2	–	39	F	–	–	–
Ctrl3	–	47	F	–	–	–
Ctrl4	–	49	M	–	–	–

possibly correlated descriptors) needs to be evaluated (Smilde et al., 2005). ASCA operates by partitioning the variation of experimental data into the contributions induced by the effect of controlled factors, usually a treatment or a condition, or of their interactions, and by analyzing the resulting matrices via simultaneous component analysis (SCA), a method similar to principal component analysis (PCA) (Smilde et al., 2005). In the case of designs involving a single factor, such as the one of the present study, ASCA starts by decomposing the variability in the experimental matrix X, according to a one-way ANOVA scheme, i.e.:

$$X = X_M + X_{Fact} + X_{Res} \quad (1)$$

where X_M is a matrix where all the rows are equal to the mean profile (grand mean) calculated across samples, X_{Fact} is the matrix accounting for the effect of the factor, which is made of the centered mean profiles corresponding to each level of the factor, and X_{Res} collects the residual variability. The entity of the effect of the controlled factor on the multivariate profile is estimated by the Frobenius norm (sum of the squared elements) of the matrix X_{Fact}, while its statistical significance is assessed using permutation tests (Vis et al., 2007). Permutation testing allows non-parametrical evaluation of the null distribution of the factor effect (i.e., of the sum of squares of the effect matrix). Operationally, it is conducted by randomly permuting the factor level labels and recalculating the ANOVA decomposition and the corresponding value of the sum of squares of X_{Fact} on the permuted data.

Interpretation of the factor effect on the multivariate data was accomplished by performing SCA, which, under the ANOVA constraints, is analogous to PCA, on the factor matrix X_{Fact}. Eventually, the residual matrix X_{Res} can be projected on the SCA model so that the resulting scores can also account for the within-level variability. First, ASCA was conducted separately for urinary and serum amino acids, inflammatory markers, and circulating fatty acids. Then, ASCA was conducted after (low-level) data fusion by integrating the information contained in individual data matrices into a single matrix (Biancolillo et al., 2019).

ComDim analysis is a multi-block version of PCA, particularly suited for assessing the relationships between individuals and variables of interest within a multi-block setting where several variables, organized in blocks, are measured in the same individuals (El Ghaziri et al., 2016). Operationally, ComDim works by extracting components that account for the maximum variance across all matrices. Assuming that the multi-block data set is made of B matrices $\{X_1, \cdots, X_b, \cdots, X_B\}$, ComDim postulates that, for each matrix, the corresponding cross-product array W_b, defined as:

$$W_b = X_b X_b^T$$

can be expressed as a weighted combination of the same set of scores Q, where the weights, also called the saliences Λ_b, are different for each block

$$W_b = Q\Lambda_b Q^T$$

Indeed, Λ_b is a diagonal matrix whose elements represent the contribution of the b^{th} block to the various components.

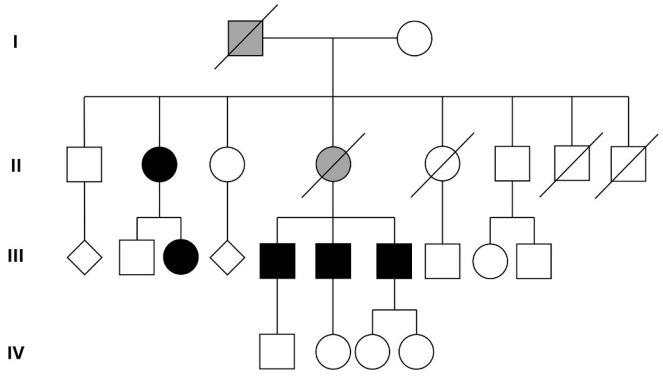

Fig. 1. Family pedigree. Charcot-Marie Tooth type 2B caused by *RAB7A* p.V162M mutation in an Italian family.

Analyses were performed using in-house routines running under MATLAB R2015b environment (The MathWorks, Natick, MA, USA).

Differences in ccf-mtDNA and MDV content are reported as mean ± standard deviation (SD). Due to the small sample size and non-normal distribution of ccf-mtDNA and MDV markers, statistical significance was determined for all experiments through Mann–Whitney U statistics. Spearman's correlation analyses were conducted to explore the relationship between ADMA, IL-1β, IL-8, and fatty acids. Analyses were performed using GraphPad Prism (Version 10.4.2) (*$p \leq 0.05$, ** $p \leq 0.01$, and *** $p \leq 0.001$).

3. Results

3.1. Characteristics of study participants

The main characteristics of CMT2B patients and controls are shown in Table 2. CMT2B_1 to CMT2B_4 patients belonged to the same Italian family carrying the *RAB7* p.V162M mutation (Colecchia et al., 2018), while CMT2B_5 harbored *RAB7* p.K126R mutation (Saveri et al., 2020).

Fig. 1 shows the family pedigree of V162M-mutated CMT2B patients. The three male probands (III-5, 6, and 7), indicated in this work as CMT2B_1, CMT2B_2 and CMT2B_4, respectively, are siblings and cousins of the only female patient (III-3) with *RAB7A* p.V162M mutation (CMT2B_3). As previously reported (Saveri et al., 2020), the K126R mutated patient inherited the *RAB7* mutation from the father, who died of acute leukemia a few months after CMT2B diagnosis.

3.2. Different ASCA models were built to explore differences in metabolic and inflammatory markers between participants with CMT2B and controls

First, ASCA models were built separately for urinary and serum amino acids, inflammatory markers, and fatty acids. ASCA models showed differences in urinary glycine and lysine, serum α-aminobutyric

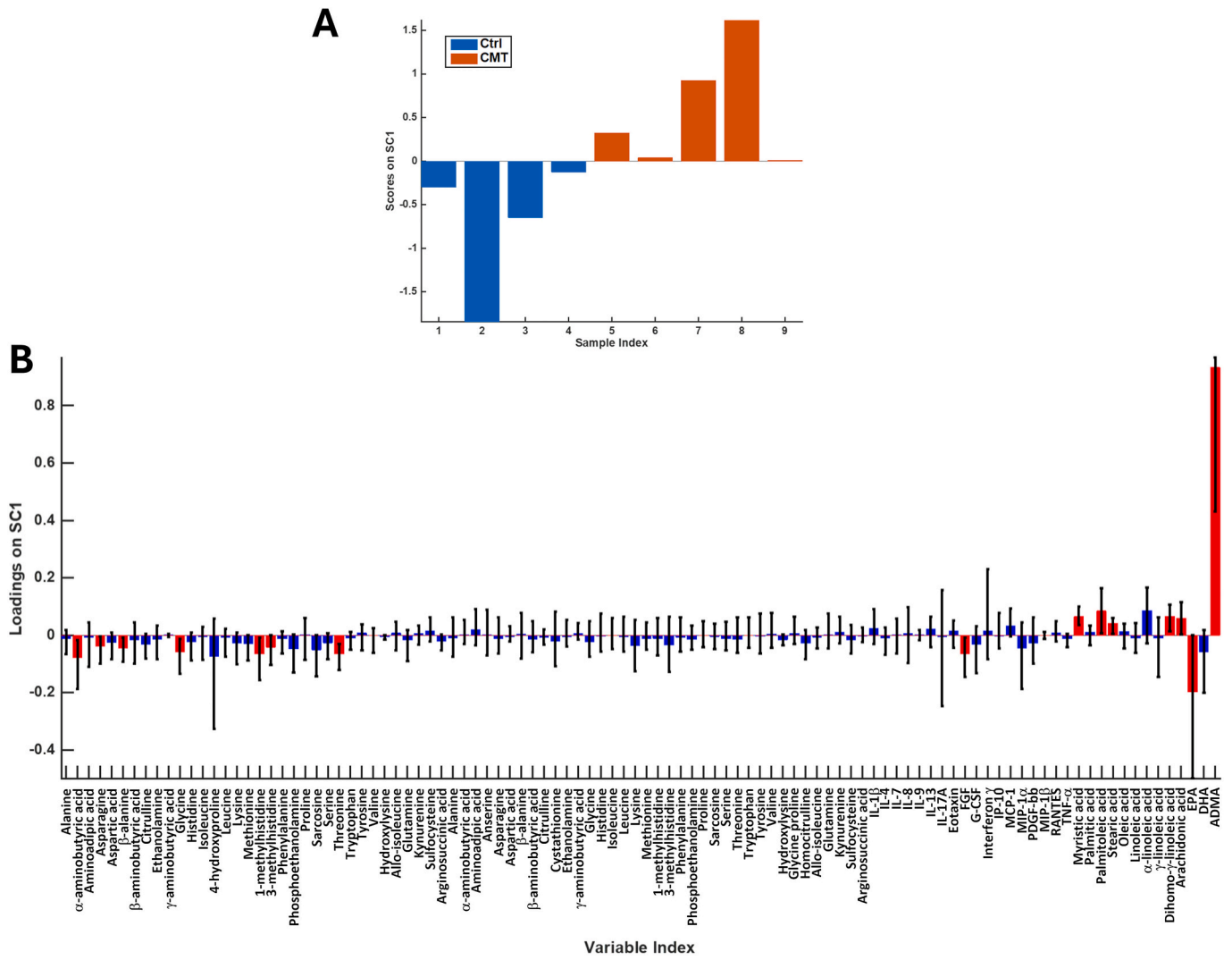

Fig. 2. ASCA model built on low-level fused data. Plots of the sample scores (A) and variable loadings (B) on the only simultaneous component (SC1) of ASCA model showing the differences in metabolic and inflammatory markers between individuals with CMT2B and controls. Variable loadings on SC1 are reported as bars with their 95 % confidence intervals. Red bars indicate variables that significantly contribute to the difference between groups. (For interpretation of the references to colour in this figure legend, the reader is referred to the web version of this article.)

acid, asparagine, β-alanine, glycine, 1-methylhistidine, threonine, arachidonic, di-homo-γ-linoleic, and myristic and palmitoleic acid between individuals with CMT2B and controls. However, permutation tests showed that differences did not reach statistical significance set at 0.05 (Supplementary information 1). Individuals with CMT2B exhibited higher serum levels of ADMA compared with controls (0.68 vs. 0.51 μM; mean difference, 0.17 μM; 95 % confidence interval (CI): 0.00 to 0.33 μM; effect size = 1.59; $p = 0.049$). Serum levels of ADMA in participants with CMT2B may suggest ongoing endothelial dysfunction and increased cardiovascular risk according to reference values proposed by leading clinical medicine laboratories (https://www.mayocliniclabs.com/api/sitecore/TestCatalog/DownloadTestCatalog?testId=607697; https://www.clevelandheartlab.com/wp-content/uploads/2018/11/CHL-D070-AUG2018-ADMA-SDMA-Practitioner-One-Pager.pdf).

ASCA model was then built on low-level fused data, i.e., by integrating the information contained in individual data matrices into a single matrix. In this model, individuals with CMT2B were separated from controls along the only simultaneous component (SC1) of the model, as evidenced by the scores plot in Fig. 2A. The inspection of loadings plots on SC1 (Fig. 2B) showed that ADMA displayed the highest SC1 loadings, which reflects its prominent role in differentiating individuals with CMT2B from controls. Other molecules that significantly contributed to separation along SC1 were arachidonic, di-homo-γ-linoleic, myristic, palmitoleic, and stearic acid (higher in CMT2B) and EPA (higher in controls). Lower levels of serum 1- and 3-methylhistidine, α- and β-aminobutyric acid, asparagine, glycine, threonine, as well as lower fibroblast growth factor (FGF) characterized the profile of individuals with CMT2B compared with controls. The permutation test assessing the significance of the results showed that the experimentally observed values of the sum of squares of the effect matrix (the ASCA equivalent of the F statistics) fell relatively close to the tail of the distribution of the same test statistics under the null hypothesis (Fig. 3), resulting in p values only slightly higher than 0.05.

The results of multi-block exploratory analysis by ComDim are shown in Fig. 4, where the scores of the samples along the first two CC of the model (accounting for almost 90 % of total variance) are reported. The plot shows that individuals with CMT2B and controls are mostly separated along CC1, the latter having on average a higher score.

The salience values for the component (supplementary Fig. S6) indicate that all blocks contributed significantly to its definition, even if the contribution of ADMA was the most relevant. Inspection of the corresponding loadings (supplementary Fig. S7) suggests higher values of ADMA in individuals with CMT2B, as well as of interleukin (IL)-1β, IL-7, IL-8, IL-9, IL-13, eotaxin, and of most fatty acids. On the other hand,

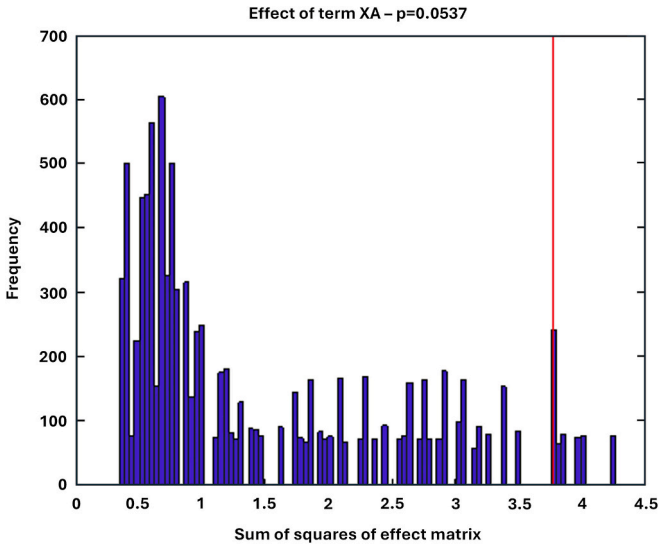

Fig. 3. Significance of the ASCA model of low-fused metabolic and inflammatory variables between participants with CMT2B and controls, as assessed by permutation tests. The experimental sum of squares (vertical red line) was compared to the distribution of the null hypothesis, estimated via permutation tests (blue histogram), resulting in a p value of 0.0537. (For interpretation of the references to colour in this figure legend, the reader is referred to the web version of this article.)

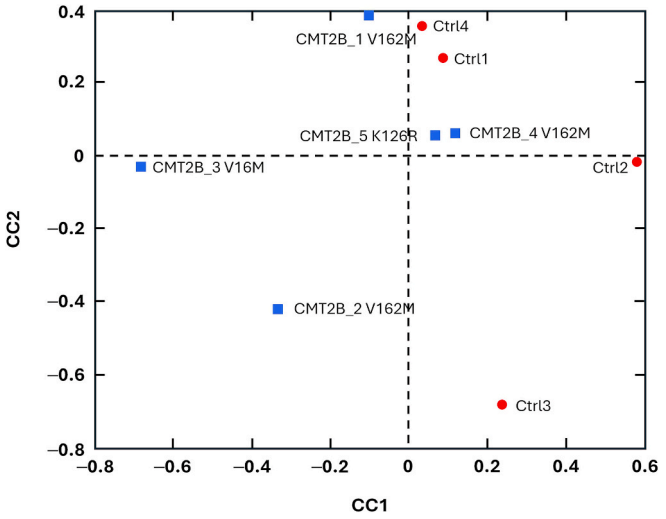

Fig. 4. Scores plot of the multi-block Common Dimensions analysis built on metabolic and inflammatory markers from individuals with CMT2B and controls. Scores of the samples along the first two common components of the model are reported. A separation between individuals with CMT2B (blue squares) and controls (red circles) is apparent along CC1. (For interpretation of the references to colour in this figure legend, the reader is referred to the web version of this article.)

controls showed higher values of linoleic and eicosapentaenoic acid, all amino acids in urine, citrulline, β-alanine, 3-methylhistidine, threonine, hydroxylysine, glycine, and α-aminobutyric acid in serum, and of interferon-induced protein 10, interferon γ, and platelet derived growth factor BB (PDGF BB).

3.3. Levels of circulating cell-free mitochondrial DNA showed no differences in CMT2B patients compared with control individuals

With the aim of understanding whether the inflammatory status of CMT2B patients was also related to mtDNA as a DAMP, we measured the ccf-mtDNA copy number in the serum of CMT2B patients and healthy controls. ddPCR was used to obtain a direct quantification of the number of copies of mtDNA in 1 μL of serum samples. No differences were observed between groups (Fig. 5). Interestingly, lower levels of ccf-mtDNA were found in the patient harboring p.K126R *RAB7* mutation (CMT2B_5) compared with controls (Ctrl2–4) and patients with p.V162M *RAB7* mutation (CMT2B_1–4).

3.4. Mitochondria-derived vesicles were differentially secreted in CMT2B patients compared with control individuals

The finding of unvaried levels of ccf-mtDNA between CMT2B patients and controls prompted us to investigate whether the inflammatory status of CMT2B patients could be related to higher release of MDVs as DAMPs. Thus, we purified EVs from CMT2B and control sera by immunoprecipitation and analyzed their mitochondrial signature by Western blot analysis (Fig. 6).

We found a higher secretion of CD63-positive EVs in the serum of all CMT2B patients (Fig. 6A-C), accompanied by increased secretion of EV-rich ATP5A (Fig. 6 A, D-E). Unexpectedly, the analysis of SDHB expression in these EVs, was significantly reduced in the sera of CMT2B patients compared to controls (Fig. 6A, H-I). Protein levels of SDHA (Fig. 6A, F-G), NDUFB8 (Fig. 6A, J-K), and CD9 (data not shown) were not different between groups.

These data suggest that alterations in the mitochondrial quality control (MQC) process exist in CMT2B patients and can be related to the mitochondrial dysfunction observed in these individuals.

3.5. Correlation analyses of ADMA, inflammatory markers, and fatty acids

Correlation analyses were run to explore the relationship between markers of inflammation, endothelial dysfunction, and fatty acid metabolism (Supplementary Table 1). Statistically significant positive correlations were found between ADMA levels and dihomo-γ-linoleic acid ($r = 0.901$, $p = 0.037$). Conversely, IL-1β was positively correlated with eicosapentaenoic acid (EPA; $r = 0.921$, $p = 0.026$). These findings indicate a potential link between ADMA-mediated endothelial dysfunction, inflammation, and lipid metabolism.

4. Discussion

To the best of our knowledge, this is the first study to quantify ccf-mtDNA and secreted MDVs, and evaluate a large number of inflammatory and metabolic markers in individuals with CMT2B. It is still unclear why a mutation in a ubiquitously expressed protein, such as RAB7, can cause functional alterations only at the neuro peripheral level. The mutation causes an alteration in the mitochondria of peripheral neurons, but not in those of the central nervous system (Gu et al., 2022). Whether this peripheral neuropathy is associated with increased levels of inflammatory markers, in conjunction with greater secretion of mtDNA and MDVs due to mitochondrial alterations, is a missing piece of knowledge that can help elucidate its pathological mechanisms and support the identification of more targeted and effective therapies.

Results of our investigation indicated that participants with CMT2B had higher levels of ADMA as well as of IL-1β, IL-8, IL-9, IL-13, eotaxin, and most fatty acids compared with controls. Lower levels of serum 1- and 3-methylhistidine, α- and β-aminobutyric acid, asparagine, glycine, threonine, and PDGF BB were found to characterize the profile of individuals with CMT2B. Although inflammatory and metabolic markers contributed significantly to defining the profile of participants with CMT2B, the contribution of ADMA was the most relevant, and ADMA was the only molecule with a difference in concentration reaching statistical significance. High concentrations of ADMA accurately reflect a patient's disease state and are implicated in axonal neurodegeneration

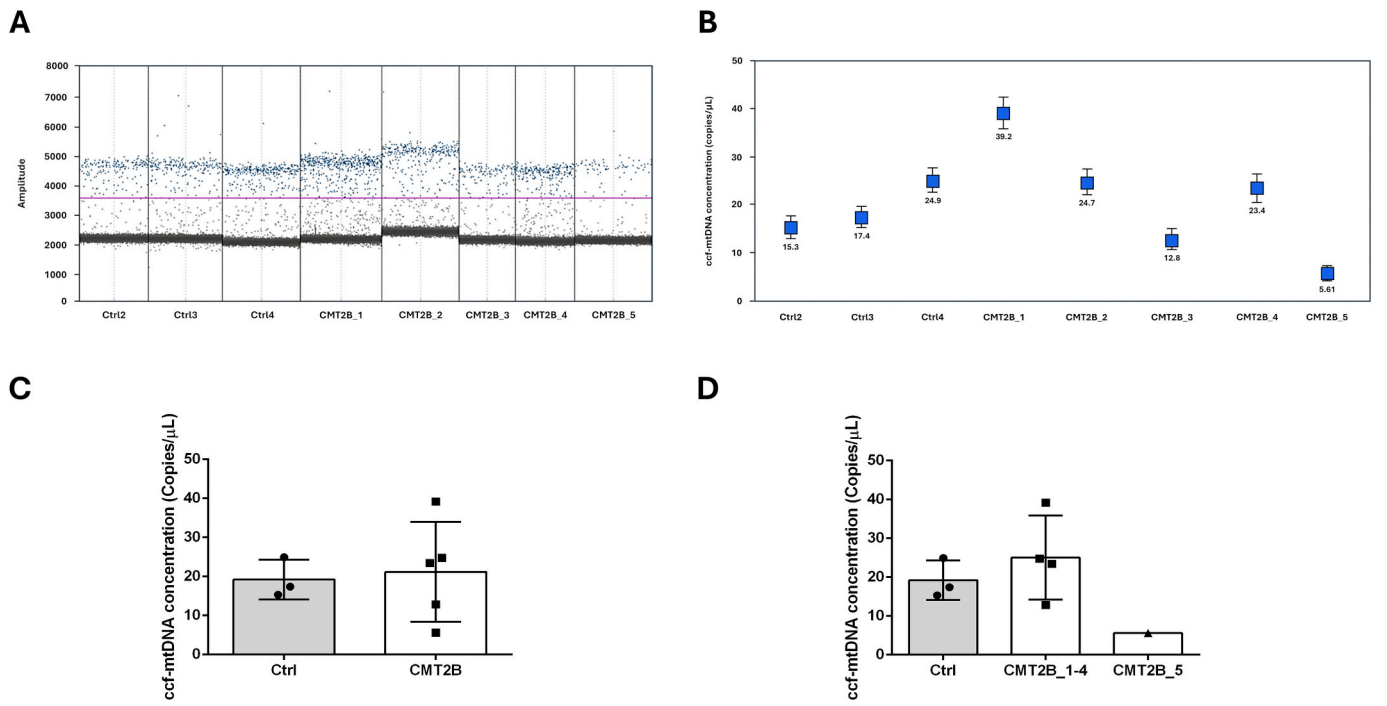

Fig. 5. (A) Representative one-dimensional circulating cell-free mtDNA (ccf-mtDNA) scatter plots obtained by analysis of serum of CMT2B patients and controls. (B) Levels of mtDNA (copies/μL) obtained in single serum samples from CMT2B patients and controls. (C) The histogram shows different concentrations of ccf-mtDNA in the two groups (Ctrl, control, and CMT2B patients). (D) The histogram represents the results of the ccf-mtDNA concentration analysis in healthy controls and CMT2B_1 to 4 (p.V162M mutated) and CMT2B_5 (p.K126R mutated) patients.

(Ikenaka et al., 2022). Excessive ADMA secretion triggers its uptake by endothelial cells where it uncouples endothelial nitric oxide synthase (eNOS) resulting in the generation of high levels of toxic peroxynitrite radical ($ONOO^-$). Being a NOS inhibitor, high serum levels of ADMA observed in CMT2B patients may indicate ongoing endothelial dysfunction and reduced mitochondrial function due to insufficient oxygen supply (Sibal et al., 2010). The positive correlation between ADMA and dihomo-γ-linoleic acid further supports this hypothesis and suggests a possible link between altered fatty acid metabolism, mitochondrial stress, and elevated ADMA. Some fatty acids are known to impair mitochondrial function (Chen et al., 2023a, 2023b). Excessive mitochondrial ROS, among other stressors, can inactivate dimethylarginine dimethylaminohydrolase1, the enzyme responsible for ADMA clearance thereby leading to accumulation of ADMA (Balasubramanian et al., 2017). In line with this are the correlations observed between ADMA and dihomo-γ-linoleic acid and between IL-1β and EPA, possibly indicating the existence of a metabolic-inflammatory axis in individuals with CMT2B. In apparent contrast, no significant differences were observed for ccf-mtDNA levels between CMT2B patients and controls. However, the patient harboring the *RAB7A* p.K126R mutation (CMT2B_5) showed lower levels of ccf-mtDNA compared with controls and those with p.V162M *RAB7* mutation (CMT2B_1–4). Moreover, we observed a significant increase in ATP5A and a significant decrease in SDHB secreted in EVs in the serum of all patients compared with controls.

Recently, it was demonstrated that *RAB7A* mutations of CMT2B were associated with alterations of mitochondrial dynamics (Gu et al., 2022; Wong et al., 2019) and dysregulated lipid metabolism (Giudetti et al., 2020). Altered autophagy was also found in individuals with CMT2B (Colecchia et al., 2018; Romano et al., 2022). Reduced mitochondrial quality due to abnormal mitochondrial dynamics and mitophagy also triggers oxidative stress (Chen et al., 2023a, 2023b). RAB7 is a small GTPase involved in controlling vesicular trafficking between endosomes and lysosomes and is instrumental in lysosomal biogenesis, intracellular distribution, and functions (Guerra and Bucci, 2016). Moreover, RAB7 regulates autophagy, mitophagy, and mitochondrial dynamics (Guerra and Bucci, 2016), likely influencing mitochondrial quality. Notably, RAB7 mediates the fusion of MDVs with late endosomes for their subsequent degradation (Matheoud et al., 2016) and is a key regulator of MDV secretion (Gagliardi et al., 2024). MDV trafficking assists with mitochondrial antigen-presentation in immune cells in the absence of the mitophagy regulators PTEN-induced kinase 1 or Parkin (Matheoud et al., 2016). In CMT2B, the existence of a proinflammatory profile and altered fatty acid homeostasis is plausible and attributable to compromised intracellular membrane trafficking.

The finding of unvaried levels of ccf-mtDNA between cases and controls was unexpected, this molecule being unloaded in the setting of damaged and low-quality organelles to alleviate the burden of mitochondrial damage (Ferrucci et al., 2024). However, there may be some explanations for this finding. Indeed, it could be a disease-specific trait indicating the inability of mtDNA unloading in the setting of severely compromised organelles and dysregulated membrane trafficking. One of the mechanisms whereby mtDNA can be unloaded is mild oxidative stress, during which cells call upon MDV generation to release portions of dysfunctional organelles, including mtDNA (Ferrucci et al., 2024). Conversely, mitochondria in individuals with CMT2B are clearly fragmented and dysfunctional (Gu et al., 2022). Another hypothesis relates to the apparent paradox that characterizes CMT2B in which an increase in lysosomal degradation activity is accompanied by autophagy dysfunction (Colecchia et al., 2018; Romano et al., 2021b). In vitro experiments showed that *RAB7* CMT2B mutants are characterized by altered nucleotide exchange and protein activation (McCray et al., 2010). Mutant proteins have a higher nucleotide dissociation rate constant (K_{off}) which confers earlier tendency to release nucleotides (GTP and GDP) compared with wild-type proteins (De Luca et al., 2008; McCray et al., 2010; Spinosa et al., 2008). The GDP K_{off} is higher than the GTP K_{off}, but the intracellular concentration of GTP is greater than GDP. The premature GDP release and a higher probability of binding GTP may explain, at least partly, why RAB7 CMT2B mutants are mainly in the GTP-bound form. However, because of increased K_{off} for GTP, this

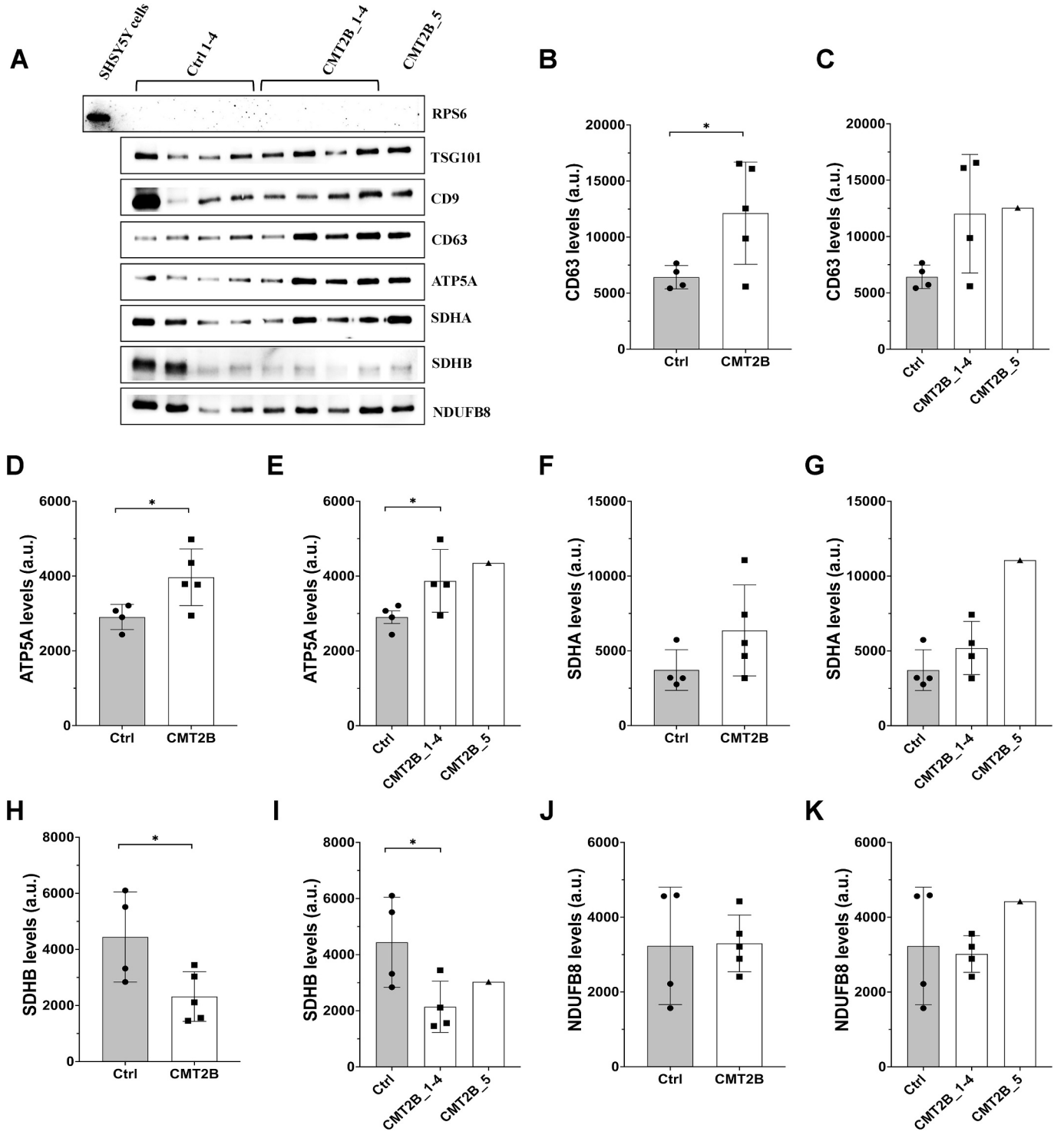

Fig. 6. (A) Extracellular vesicles (EVs) were purified by immunoisolation. Positive (TSG101, CD63 and CD9) and negative controls (RPS6) were used to verify the purity of EVs. Mitochondrial protein level was evaluated in EVs by Western blot analysis. (B—K) The histograms show different relative abundance of CD63, ATP5A, SDHB, SDHA, NDUFB8 in the two groups (Ctrl, control, and CMT2B patients) and in healthy controls and CMT2B_1 to 4 (p.V162M mutated) and CMT2B_5 (p.K126R mutated) patients determined through densitometric analysis normalized against total serum protein content. Data represent the mean ± SD of at least three independent experiments (* $p < 0.05$; ** $p < 0.01$; ***$p < 0.001$).

nucleotide can also be released prematurely, negatively affecting the GTPase activity per binding event (De Luca et al., 2008; McCray et al., 2010; Spinosa et al., 2008). Hence, depending on the kinetic requirements of the regulated process, mutant RAB7 proteins may behave as active or inhibitory mutants. This hypothesis could justify a mechanistic bivalent action of RAB7 in endosomal trafficking whereby either an increase in RAB7-related lysosomal degradation or autophagy slowdown have been described in CMT2B (Colecchia et al., 2018; Romano et al., 2021b). Higher lysosomal function and dysfunctional autophagy were observed in skin fibroblasts of patients used in the present work (Romano et al., 2021b).

A direct action of RAB7 was also described in mitophagy regulation

(Yamano et al., 2014), and it is reasonable to suppose that dysfunctional autophagy may impair mitophagy. Furthermore, we have recently demonstrated that impairment of RAB7, affecting lysosomal function and biogenesis in the setting of mitochondrial deficit, makes the cells unable to trigger MDV degradation as part of the MQC machinery (Gagliardi et al., 2024). Hence, the inability to degrade damaged mitochondrial particles is compensated by increased MDV secretion as part of MQC process (Gagliardi et al., 2024).

Based on these observations, it is possible that the MQC system, particularly mitophagy, is unable to eliminate dysfunctional organelles in CMT2B. However, an increase in lysosomal-mediated MDV degradation, according to the described disease-associated increase in lysosomal function (Romano et al., 2021b), could compensate for these alterations in an effort to restore mitochondrial homeostasis. This scenario is in line with our findings of reduced SDHB encapsulated in MDVs, probably due to an increase in lysosomal degradation of these vesicles, and no differences in secreted SDHA and NDUFB8 or in ccf-mtDNA. It is also possible that the lack of significant differences in ccf-mtDNA levels in participants with CMT2B was due to limitations in our experimental approach, which did not distinguish between EV-encapsulated mtDNA and ccf-mtDNA. Our method measured the total amount of extracellular mtDNA, encompassing both freely circulating and EV-associated forms. Therefore, we cannot exclude the possibility that differences would emerge if those two mtDNA fractions were analyzed separately. It should also be considered that EV-encapsulated mtDNA is subject to lysosomal degradation, potentially exacerbated by dysregulated RAB7-mediated fusion of MDVs with lysosomes (Gagliardi et al., 2024; Romano et al., 2021b). Moreover, under stress conditions, mtDNA can be directed to endosomes and subsequently degraded in lysosomes independently of MDVs (Kakanj et al., 2025). These pathways may contribute to the absence of statistically significant differences in ccf-mtDNA levels, beyond any methodological limitations, and warrant further investigation in future studies. On the other hand, higher ATP5A levels have been identified and may be explained as the result of an escape mechanism from lysosomal degradation, possibly due to the extent of mitochondrial damage, and its consequent secretion in CD63-positive EVs. Notably, CD63, also known as lysosome-associated membrane protein-3, is a marker of multivesicular bodies, and its presence in EVs and MDVs indicates their endosomal origin (Palmulli et al., 2024).

Finally, a broader explanation for the lack of significant differences in ccf-mtDNA levels as well as in other biomolecular findings may lie in an inherent and unavoidable limitation of our study related to the small sample size. This limitation reduces statistical power, particularly in detecting subtle differences, and impacts the generalizability of findings to the whole population with CMT2B.

However, it is important to note that CMT2B is an exceptionally rare subtype of the already rare CMT disease. Our study reached its feasible maximum, as the cohort included the only two Italian families currently identified with *RAB7* V162M or *RAB7* K126R mutations (Manganelli et al., 2012; Saveri et al., 2020). While this reflects a comprehensive effort given the disease's rarity, we acknowledge that the limited sample size impacts the robustness and interpretation of results. This limitation is particularly relevant in the context of findings such as the non-significant differences in ccf-mtDNA levels, which may be influenced not only by methodological constraints but also by interindividual variability and limited statistical power. Future longitudinal studies with larger and more genetically diverse cohorts will be essential to validate and extend our observations.

Finally, the collection of longitudinal samples, which would have enabled moderation analyses and a more detailed characterization of the relationship between ccf-mtDNA and inflammatory and metabolic markers, was not feasible at this time. Nevertheless, we employed advanced analytical techniques and statistical modeling to extract meaningful patterns from the available data. These approaches helped offset some of the constraints and allowed us to provide novel insights into the molecular underpinnings of CMT2B.

5. Conclusion

In this study, for the first time, we analyzed mitochondria-derived components (i.e., ccf-mtDNA and MDVs) along with inflammatory and metabolic markers in the serum of patients with CMT2B. Our findings reveal altered MDV trafficking and elevated serum levels of ADMA in individuals with CMT2B, providing new insights into disease pathophysiology. While mitochondrial abnormalities in fibroblasts from the same patients have been previously reported, the concurrent presence of altered endosomal trafficking, mitochondrial dysfunction, and endothelial impairment represents a novel observation that warrants further investigation. Therefore, our findings may serve as a foundation for elucidating the mechanisms driving abnormal vesicular secretion in this specific metabolic context and could ultimately inform the development of more targeted therapeutic strategies.

CRediT authorship contribution statement

Giulia Girolimetti: Writing – original draft, Methodology, Investigation, Conceptualization. **Federico Marini:** Software, Formal analysis. **Riccardo Calvani:** Investigation. **Hélio José Coelho-Júnior:** Investigation. **Jacopo Gervasoni:** Methodology. **Lavinia Santucci:** Methodology. **Stefano Tozza:** Investigation, Conceptualization. **Fiore Manganelli:** Investigation, Conceptualization. **Paola Saveri:** Investigation, Conceptualization. **Davide Pareyson:** Investigation, Conceptualization. **Emanuele Marzetti:** Writing – review & editing, Supervision, Funding acquisition. **Cecilia Bucci:** Writing – review & editing, Supervision, Conceptualization. **Anna Picca:** Writing – original draft, Methodology, Investigation, Conceptualization. **Flora Guerra:** Writing – original draft, Validation, Investigation, Conceptualization.

Ethical standards

The study was approved by the Ethics Committee of Azienda Ospedaliera Universitaria "Federico II" (Naples, Italy) and the National Institute of Health (Baltimore, MD, USA), and was therefore performed in accordance with the ethical standards laid down in the 1964 Declaration of Helsinki and its later amendments. All persons gave their informed consent prior to the inclusion in the study.

Declaration of competing interest

The authors declare no conflicts of interest.

Acknowledgments

The article processing charge was funded by the Italian Ministry of Health (Ricerca Corrente 2025).

Appendix A. Supplementary data

Supplementary data to this article can be found online at https://doi.org/10.1016/j.nbd.2025.107051.

Data availability

Data will be made available upon request to the corresponding authors.

References

Balasubramanian, V., Mehta, G., Jones, H., Sharma, V., Davies, N.A., Jalan, R., Mookerjee, R.P., 2017. Post-transcriptional regulation of hepatic DDAH1 with TNF blockade leads to improved eNOS function and reduced portal pressure in cirrhotic rats. Sci. Rep. 7, 17900. https://doi.org/10.1038/s41598-017-18094-3.

Biancolillo, A., Boqué, R., Cocchi, M., Marini, F., 2019. Data fusion strategies in food analysis. In: Cocchi, M. (Ed.), Data Handling in Science and Technology. Elsevier Ltd, Oxford, pp. 271–310. https://doi.org/10.1016/B978-0-444-63984-4.00010-7.

Bucci, C., Frunzio, R., Chiariotti, L., Brown, A.L., Rechler, M.M., Bruni, C.B., 1988. A new member of the ras gene superfamily identified in a rat liver cell line. Nucleic Acids Res. 16, 9979–9993. https://doi.org/10.1093/NAR/16.21.9979.

Bucci, C., Bakke, O., Progida, C., 2012. Charcot-Marie-tooth disease and intracellular traffic. Prog. Neurobiol. 99, 191–225. https://doi.org/10.1016/J.PNEUROBIO.2012.03.003.

Chavrier, P., Parton, R.G., Hauri, H.P., Simons, K., Zerial, M., 1990. Localization of low molecular weight GTP binding proteins to exocytic and endocytic compartments. Cell 62, 317–329. https://doi.org/10.1016/0092-8674(90)90369-P.

Chen, L., Zhang, Q., Meng, Y., Zhao, T., Mu, C., Fu, C., Deng, C., Feng, J., Du, S., Liu, W., Geng, G., Ma, K., Cheng, H., Liu, Q., Luo, Q., Zhang, J., Du, Z., Cao, L., Wang, H., Liu, Y., Lin, J., Chen, G., Liu, L., Lam, S.M., Shui, G., Zhu, Y., Chen, Q., 2023a. Saturated fatty acids increase LPI to reduce FUNDC1 dimerization and stability and mitochondrial function. EMBO Rep. 24, e54731. https://doi.org/10.15252/embr.202254731.

Chen, W., Zhao, H., Li, Y., 2023b. Mitochondrial dynamics in health and disease: mechanisms and potential targets. Signal Transduct. Target. Ther. 8, 333. https://doi.org/10.1038/S41392-023-01547-9.

Colecchia, D., Stasi, M., Leonardi, M., Manganelli, F., Nolano, M., Veneziani, B.M., Santoro, L., Eskelinen, E.L., Chiariello, M., Bucci, C., 2018. Alterations of autophagy in the peripheral neuropathy Charcot-Marie-tooth type 2B. Autophagy 14, 930–941. https://doi.org/10.1080/15548627.2017.1388475.

De Luca, A., Progida, C., Spinosa, M.R., Alifano, P., Bucci, C., 2008. Characterization of the Rab7K157N mutant protein associated with Charcot-Marie-tooth type 2B. Biochem. Biophys. Res. Commun. 372, 283–287. https://doi.org/10.1016/j.bbrc.2008.05.060.

Dong, H., Qin, B., Zhang, H., Lei, L., Wu, S., 2024. Current treatment methods for Charcot-Marie-tooth diseases. Biomolecules 14, 1138. https://doi.org/10.3390/BIOM14091138.

El Ghaziri, A., Cariou, V., Rutledge, D.N., Qannari, E.M., 2016. Analysis of multiblock datasets using ComDim: overview and extension to the analysis of (K + 1) datasets. J. Chemom. 30, 420–429. https://doi.org/10.1002/CEM.2810.

Ferrucci, L., Guerra, F., Bucci, C., Marzetti, E., Picca, A., 2024. Mitochondria break free: mitochondria-derived vesicles in aging and associated conditions. Ageing Res. Rev. 102, 102549. https://doi.org/10.1016/J.ARR.2024.102549.

Gagliardi, S., Mitruccio, M., Di Corato, R., Romano, R., Aloisi, A., Rinaldi, R., Alifano, P., Guerra, F., Bucci, C., 2024. Defects of mitochondria-lysosomes communication induce secretion of mitochondria-derived vesicles and drive chemoresistance in ovarian cancer cells. Cell Commun. Signal 22, 165. https://doi.org/10.1186/s12964-024-01507-y.

Giudetti, A.M., Guerra, F., Longo, S., Beli, R., Romano, R., Manganelli, F., Nolano, M., Mangini, V., Santoro, L., Bucci, C., 2020. An altered lipid metabolism characterizes Charcot-Marie-tooth type 2B peripheral neuropathy. Biochim. Biophys. Acta Mol. Cell Biol. Lipids 1865, 158805. https://doi.org/10.1016/J.BBALIP.2020.158805.

Gu, Y., Guerra, F., Hu, M., Pope, A., Sung, K., Yang, W., Jetha, S., Shoff, T.A., Gunatilake, T., Dahlkamp, O., Shi, L.Z., Manganelli, F., Nolano, M., Zhou, Y., Ding, J., Bucci, C., Wu, C., 2022. Mitochondria dysfunction in Charcot Marie tooth 2B peripheral sensory neuropathy. Commun. Biol. 5, 717. https://doi.org/10.1038/S42003-022-03632-1.

Guerra, F., Bucci, C., 2016. Multiple roles of the small GTPase Rab7. Cells 5, 34. https://doi.org/10.3390/cells5030034.

Houlden, H., King, R.H.M., Muddle, J.R., Warner, T.T., Reilly, M.M., Orrell, R.W., Ginsberg, L., 2004. A novel RAB7 mutation associated with ulcero-mutilating neuropathy. Ann. Neurol. 56, 586–590. https://doi.org/10.1002/ANA.20281.

Ikenaka, K., Maeda, Y., Hotta, Y., Nagano, S., Yamada, S., Ito, D., Torii, R., Kakuda, K., Tatebe, H., Atsuta, N., Aguirre, C., Kimura, Y., Baba, K., Tokuda, T., Katsuno, M., Kimura, K., Sobue, G., Mochizuki, H., 2022. Serum asymmetric dimethylarginine level correlates with the progression and prognosis of amyotrophic lateral sclerosis. Eur. J. Neurol. 29, 1410–1416. https://doi.org/10.1111/ENE.15254.

Kakanj, P., Bonse, M., Kshirsagar, A., Gökmen, A., Gaedke, F., Sen, A., Mollá, B., Vogelsang, E., Schauss, A., Wodarz, A., Pla-Martín, D., 2025. Retromer promotes the lysosomal turnover of mtDNA. Sci. Adv. 11, eadr6415. https://doi.org/10.1126/sciadv.adr6415.

Kepp, O., Galluzzi, L., Kroemer, G., 2011. Mitochondrial control of the NLRP3 inflammasome. Nat. Immunol. 12, 199–200. https://doi.org/10.1038/ni0311-199.

Lin, M., Liu, N., Qin, Z., Wang, Y., 2022. Mitochondrial-derived damage-associated molecular patterns amplify neuroinflammation in neurodegenerative diseases. Acta Pharmacol. Sin. 43, 2439–2447. https://doi.org/10.1038/S41401-022-00879-6.

Manganelli, F., Pisciotta, C., Provitera, V., Taioli, F., Iodice, R., Topa, A., Fabrizi, G.M., Nolano, M., Santoro, L., 2012. Autonomic nervous system involvement in a new CMT2B family. J. Peripher. Nerv. Syst. 17, 361–364. https://doi.org/10.1111/J.1529-8027.2012.00415.X.

Matheoud, D., Sugiura, A., Bellemare-Pelletier, A., Laplante, A., Rondeau, C., Chemali, M., Fazel, A., Bergeron, J.J., Trudeau, L.E., Burelle, Y., Gagnon, E., McBride, H.M., Desjardins, M., 2016. Parkinson's disease-related proteins PINK1 and Parkin repress mitochondrial antigen presentation. Cell 166, 314–327. https://doi.org/10.1016/j.cell.2016.05.039.

Mayne, K., White, J.A., McMurran, C.E., Rivera, F.J., de la Fuente, A.G., 2020. Aging and neurodegenerative disease: is the adaptive immune system a friend or foe? Front. Aging Neurosci. 12, 572090. https://doi.org/10.3389/FNAGI.2020.572090.

McCray, B.A., Skordalakes, E., Taylor, J.P., 2010. Disease mutations in Rab7 result in unregulated nucleotide exchange and inappropriate activation. Hum. Mol. Genet. 19, 1033–1047. https://doi.org/10.1093/hmg/ddp567.

Meggouh, F., Bienfait, H.M.E., Weterman, M.A.J., De Visser, M., Baas, F., 2006. Charcot-Marie-tooth disease due to a de novo mutation of the RAB7 gene. Neurology 67, 1476–1478. https://doi.org/10.1212/01.WNL.0000240068.21499.F5.

Palmulli, R., Couty, M., Piontek, M.C., Ponnaiah, M., Dingli, F., Verweij, F.J., Charrin, S., Tantucci, M., Sasidharan, S., Rubinstein, E., Kontush, A., Loew, D., Lhomme, M., Roos, W.H., Raposo, G., van Niel, G., 2024. CD63 sorts cholesterol into endosomes for storage and distribution via exosomes. Nat. Cell Biol. 26, 1093–1109. https://doi.org/10.1038/s41556-024-01432-9.

Pareyson, D., Marchesi, C., 2009. Diagnosis, natural history, and management of Charcot-Marie-tooth disease. Lancet Neurol. 8, 654–667. https://doi.org/10.1016/S1474-4422(09)70110-3.

Picca, A., Calvani, R., Coelho-Junior, H.J., Landi, F., Bernabei, R., Marzetti, E., 2020a. Mitochondrial dysfunction, oxidative stress, and neuroinflammation: intertwined roads to neurodegeneration. Antioxidants 9, 647. https://doi.org/10.3390/antiox9080647.

Picca, A., Guerra, F., Calvani, R., Coelho-Júnior, H.J., Landi, F., Bernabei, R., Romano, R., Bucci, C., Marzetti, E., 2020b. Extracellular vesicles and damage-associated molecular patterns: a Pandora's box in health and disease. Front. Immunol. 11, 601740. https://doi.org/10.3389/FIMMU.2020.601740.

Podlesniy, P., Trullas, R., 2018. Biomarkers in cerebrospinal fluid: analysis of cell-free circulating mitochondrial DNA by digital PCR. Methods Mol. Biol. 1768, 111–126. https://doi.org/10.1007/978-1-4939-7778-9_7.

Romano, R., Calcagnile, M., Margiotta, A., Franci, L., Chiariello, M., Alifano, P., Bucci, C., 2021a. RAB7A regulates vimentin phosphorylation through AKT and PAK. Cancers 13, 2220. https://doi.org/10.3390/cancers13092220.

Romano, R., Rivellini, C., De Luca, M., Tonlorenzi, R., Beli, R., Manganelli, F., Nolano, M., Santoro, L., Eskelinen, E.L., Previtali, S.C., Bucci, C., 2021b. Alteration of the late endocytic pathway in Charcot-Marie-tooth type 2B disease. Cell. Mol. Life Sci. 78, 351–372. https://doi.org/10.1007/s00018-020-03510-1.

Romano, R., Del Fiore, V.S., Saveri, P., Palamà, I.E., Pisciotta, C., Pareyson, D., Bucci, C., Guerra, F., 2022. Autophagy and lysosomal functionality in CMT2B fibroblasts carrying the RAB7K126R mutation. Cells 11, 496. https://doi.org/10.3390/CELLS11030496.

Santucci, L., Lomuscio, S., Primiano, A., Calvani, R., Persichilli, S., Iavarone, F., Picca, A., Canu, F., Urbani, A., Gervasoni, J., 2023. Development of a novel ultra performance liquid chromatography tandem-mass spectrometry (UPLC-MS/MS) method to measure l-arginine metabolites in plasma. Clin. Chim. Acta 543, 117306. https://doi.org/10.1016/J.CCA.2023.117306.

Saveri, P., De Luca, M., Nisi, V., Pisciotta, C., Romano, R., Piscosquito, G., Reilly, M.M., Polke, J.M., Cavallaro, T., Maria Fabrizi, G., Fossa, P., Cichero, E., Lombardi, R., Lauria, G., Magri, S., Taroni, F., Pareyson, D., Bucci, C., 2020. Charcot-Marie-tooth type 2B: a new phenotype associated with a novel RAB7A mutation and inhibited EGFR degradation. Cells 9, 1028. https://doi.org/10.3390/CELLS9041028.

Sibal, L., Agarwal, C., S., D Home, P., H Boger, R, 2010. The role of asymmetric dimethylarginine (ADMA) in endothelial dysfunction and cardiovascular disease. Curr. Cardiol. Rev. 6, 82–90. https://doi.org/10.2174/157340310791162659.

Smilde, A.K., Jansen, J.J., Hoefsloot, H.C.J., Lamers, R.J.A.N., van der Greef, J., Timmerman, M.E., 2005. ANOVA-simultaneous component analysis (ASCA): a new tool for analyzing designed metabolomics data. Bioinformatics 21, 3043–3048. https://doi.org/10.1093/BIOINFORMATICS/BTI476.

Spinosa, M.R., Progida, C., De Luca, A., Colucci, A.M., Alifano, P., Bucci, C., 2008. Functional characterization of Rab7 mutant proteins associated with Charcot-Marie-tooth type 2B disease. J. Neurosci. 28, 1640–1648. https://doi.org/10.1523/JNEUROSCI.3677-07.2008.

Tazir, M., Hamadouche, T., Nouioua, S., Mathis, S., Vallat, J.M., 2014. Hereditary motor and sensory neuropathies or Charcot-Marie-tooth diseases: an update. J. Neurol. Sci. 347, 14–22. https://doi.org/10.1016/J.JNS.2014.10.013.

Verhoeven, K., De Jonghe, P., Coen, K., Verpoorten, N., Auer-Grumbach, M., Kwon, J.M., FitzPatrick, D., Schmedding, E., De Vriendt, E., Jacobs, A., Van Gerwen, V., Wagner, K., Hartung, H.P., Timmerman, V., 2003. Mutations in the small GTP-ase late endosomal protein RAB7 cause Charcot-Marie-tooth type 2B neuropathy. Am. J. Hum. Genet. 72, 722–727. https://doi.org/10.1086/367847.

Vis, D.J., Westerhuis, J.A., Smilde, A.K., van der Greef, J., 2007. Statistical validation of megavariate effects in ASCA. BMC Bioinformat. 8, 322. https://doi.org/10.1186/1471-2105-8-322.

Wang, X., Han, C., Liu, W., Wang, P., Zhang, X., 2014. A novel RAB7 mutation in a Chinese family with Charcot-Marie-tooth type 2B disease. Gene 534, 431–434. https://doi.org/10.1016/j.gene.2013.

Welsh, J.A., Goberdhan, D.C.I., O'Driscoll, L., Buzas, E.I., Blenkiron, C., Bussolati, B., Cai, H., Di Vizio, D., Driedonks, T.A.P., Erdbrügger, U., Falcon-Perez, J.M., Fu, Q.L., Hill, A.F., Lenassi, M., Lim, S.K., Mahoney, M.G., Mohanty, S., Möller, A., Nieuwland, R., Ochiya, T., Sahoo, S., Torrecilhas, A.C., Zheng, L., Zijlstra, A., Abuelreich, S., Bagabas, R., Bergese, P., Bridges, E.M., Brucale, M., Burger, D., Carney, R.P., Cocucci, E., Crescitelli, R., Hanser, E., Harris, A.L., Haughey, N.J., Hendrix, A., Ivanov, A.R., Jovanovic-Talisman, T., Kruh-Garcia, N.A., Ku'ulei-Lyn Faustino, V., Kyburz, D., Lässer, C., Lennon, K.M., Lötvall, J., Maddox, A.L., Martens-Uzunova, E.S., Mizenko, R.R., Newman, L.A., Ridolfi, A., Rohde, E., Rojalin, T., Rowland, A., Saftics, A., Sandau, U.S., Saugstad, J.A., Shekari, F., Swift, S., Ter-Ovanesyan, D., Tosar, J.P., Useckaite, Z., Valle, F., Varga, Z., van der Pol, E., van Herwijnen, M.J.C., Wauben, M.H.M., Wehman, A.M., Williams, S., Zendrini, A., Zimmerman, A.J., Consortium, M.I.S.E.V., Théry, C., Witwer, K.W., 2024. Minimal information for studies of extracellular vesicles (MISEV2023): from basic to

advanced approaches. J. Extracell Vesicles 13, e12404. https://doi.org/10.1002/jev2.12404.
Wong, Y.C., Peng, W., Krainc, D., 2019. Lysosomal regulation of inter-mitochondrial contact fate and motility in Charcot-Marie-tooth type 2. Dev. Cell 50, 339–354.e4. https://doi.org/10.1016/J.DEVCEL.2019.05.033.
Yamano, K., Fogel, A.I., Wang, C., van der Bliek, A.M., Youle, R.J., 2014. Mitochondrial Rab GAPs govern autophagosome biogenesis during mitophagy. Elife 3, e01612. https://doi.org/10.7554/eLife.01612.